01 Nov 2001

Size-Induced Lattice Relaxation in CeO_2 Nanoparticles

X.-D. Zhou
Missouri University of Science and Technology

Wayne Huebner
Missouri University of Science and Technology, huebner@mst.edu

Size-induced lattice relaxation in CeO_2 nanoparticles

X.-D. Zhou[a] and W. Huebner
Department of Ceramic Engineering, University of Missouri-Rolla, Rolla, Missouri 65409

(Received 2 July 2001; accepted for publication 28 September 2001)

Size-induced lattice relaxation was observed for nanoscale CeO_2 single crystals with an average size from 4 to 60 nm. Results showed the finest crystallites exhibited no strain-induced line broadening, while high temperature annealing resulted in larger grain sizes and significant strains. The observed shift in the x-ray diffraction lattice parameters was assumed to be due to the formation of defects on the lattice, specifically oxygen vacancies. Modeling revealed that the oxygen vacancy concentration ($[V_O^{\bullet\bullet}]$) was found to be $\approx 4\times 10^{20}/\mathrm{cm}^3$ for the 4 nm crystallites, and decreased two orders of magnitude for larger 60 nm single crystals. © *2001 American Institute of Physics.*
[DOI: 10.1063/1.1419235]

Size-dependent ($\leqslant$50 nm) chemical and physical properties of electronic materials have been attributed primarily to either *intrinsic contributions*, such as changes in the lattice energy and discrete energy eigenstates, or *extrinsic contributions*, such as unsaturated bonding of the surface atoms.[1] Surface factors can be interpreted as ''surface relaxation,'' which has been studied in ferroelectrics ($BaTiO_3$ and $PbTiO_3$)[2] and CuO.[3] CeO_2 was chosen for study in this work since it exhibits a stable fluorite structure for a wide range of crystal sizes[4] and dopant levels.[5] In particular, the use and modeling of nanometer scale CeO_2 in the fields of catalysis, superionic conductors, solid oxide fuel cells, and polishing media for electronic devices[6] prompted further exploration to understand anomalous observations of size-dependent behavior. In most of these applications, the redox reaction between Ce^{4+} and Ce^{3+} contributes to the unique property of CeO_2. Therefore, it is interesting to study the size-dependent lattice relaxation and determine the Ce^{3+} ratio in the nanometer CeO_2 crystals.

A semibatch reactor was used to synthesize the nanometer CeO_2 single crystals at room temperature.[6] CeO_2 particles prepared in this manner exhibited the fluorite structure, as determined by x-ray diffraction (XRD), electron diffraction and lattice imaging. The particle size was varied by annealing at temperatures up to 800 °C. Typical XRD patterns for the CeO_2 nanocrystals are shown in Fig. 1; all peaks for each sample were significantly broadened resulting from size and/or strain.[7]

Williamson–Hall plots were used to separate the effects of size and strain in the nanocrystals, using the equation

$$\beta_{\mathrm{Total}}=\beta_{\mathrm{Size}}+\beta_{\mathrm{Strain}}=\frac{0.9\lambda}{t\cos\theta}+\frac{4(\Delta d)\sin\theta}{d\cos\theta}, \qquad (1)$$

where β_{total} is the full width half maximum of the XRD peak, λ is the incident x-ray wave length, θ is the diffraction angle, t is the crystal size, and Δd is the difference of the d spacing corresponding to a typical peak. A plot of $\beta_{\mathrm{total}}\cos(\theta)$ vs $4\sin(\theta)$ yields the crystal size from the intercept value, and the strain ($\Delta d/d$) from the slope. The Williamson–Hall method assumes that the diffraction peaks follow a Lorentzian distribution, shown in Fig. 1. Diffraction angles were measured from 20° to 130°, which includes ten peaks for CeO_2. The diffraction patterns (1–4) in Fig. 1 are the as-synthesized samples annealed at 150, 300, 600 and 800 °C, respectively. The size determined from the XRD results is called the x-ray coherence length (XRCL), which is interpreted as the primary crystal size in the materials. The particle size can also be calculated from the surface area data by $d_{\mathrm{BET}}=6/(\mathrm{SSA}\cdot\rho)$, where SSA is the specific surface area (m^2/g), ρ is the density of the materials (g/cm^3), and the d_{BET} is the particle size (μm). Table I contains the results of these calculations; the nearly identical sizes indicate the CeO_2 particles are single crystals.

The transmission electron microscopy (TEM) image (Fig. 2) shows the typical lattice image of the nanocrystals along the [111] direction. The spacing of the lattice fringes apparent in the core of the crystallites matches the XRD results. That said, the surface of most of the crystallites ap-

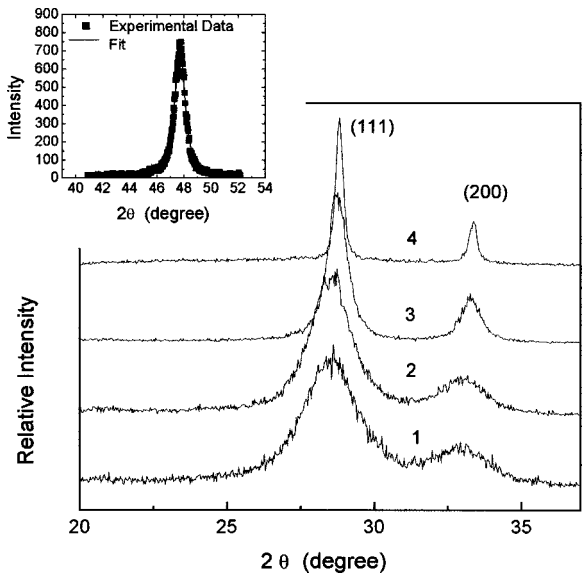

FIG. 1. Typical x-ray diffraction patterns at different annealing temperatures 1:150 °C, 2:300 °C, 3:600 °C, 4:800 °C. Inset figure is an example of Lorentzian fit of an x-ray diffraction peak.

[a]Author to whom correspondence should be addressed; electronic mail: zhou@umr.edu

TABLE I. Comparison of CeO_2 particle size as determined by XRD and BET.

Pattern number	1	2	3	4
Annealing T (°C)	150	300	600	800
XRCL (nm)	3.9	4.3	12.5	60.3
BET (nm)	5.0	5.9	12	60

pears disordered, or even amorphous. The latter provides a large driving force for ordering through lattice and surface diffusion, with a low activation energy of 2.4 kJ/mol.[7]

The Williamson–Hall plots for the CeO_2 crystals are shown in Figs. 3 and 4. For the CeO_2 with an average size (XRCL) of 3.9 and 4.3 nm, the absence of any slope is indicative of no internal strain. In these samples then, the line broadening is due to just size effects. The analysis of the larger CeO_2 shown in Fig. 4 exhibits a clear contribution of strain effects. Upon high temperature annealing and subsequent crystal growth, significant strain is present along crystalline boundaries due to lattice mismatch. This is similar to grain boundaries in sintered ceramics.

Another interesting observation shown in Fig. 1 is the peak shift with crystal size. In the case of the finer crystal size, the peak was shifted to smaller 2θ angles, corresponding to a larger d spacing. The lattice parameters for each crystallite size were determined from the high angle diffraction peaks, in which the Cu $K\alpha 1$ from $K\alpha 2$ can be clearly separated. In this research, XRD data over $85° \leqslant 2\theta \leqslant 130°$ were collected; this includes six diffraction planes. The lattice parameter of the samples annealed at 800 °C was assumed as the standard in this experiment. Results of these calculations are shown in Fig. 5.

Recently Tsunekawa *et al.*[8] studied the influence of particle size on the Ce^{3+}/Ce^{4+} ratio in CeO_2 nanoparticles. In their work, a higher concentration of Ce^{3+} was present in the finer particle sizes. The expansion of the lattice with decreasing particle size observed in this work complements Tsunekawa *et al.*[8] if the assumption is made that the lattice expansion is due to the presence of a larger concentration of

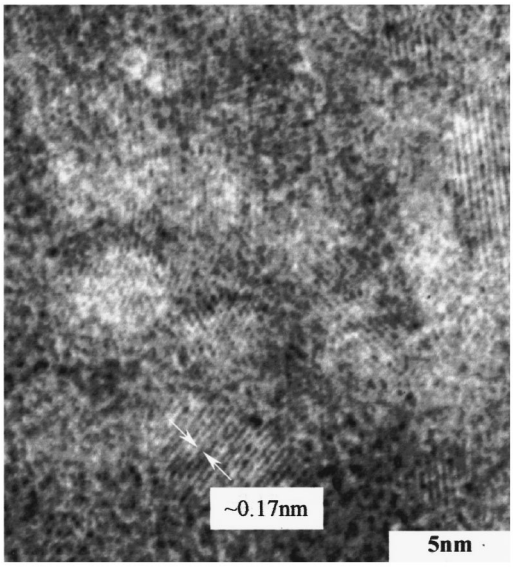

FIG. 2. Lattice fringe image of CeO_2 annealing at 150 °C.

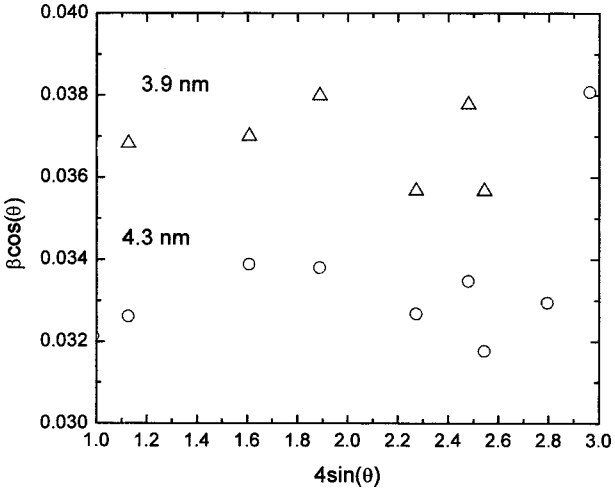

FIG. 3. Williamson–Hall plot of the CeO_2 powders with different crystal sizes.

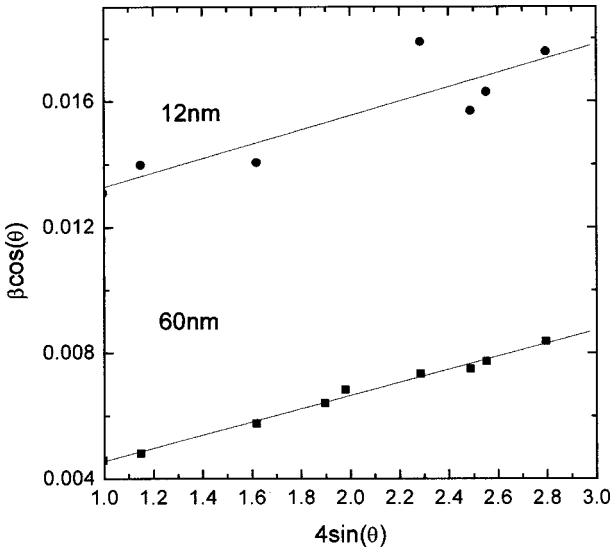

FIG. 4. Williamson–Hall plot of the CeO_2 crystals with different crystal sizes of 12 and 60 nm.

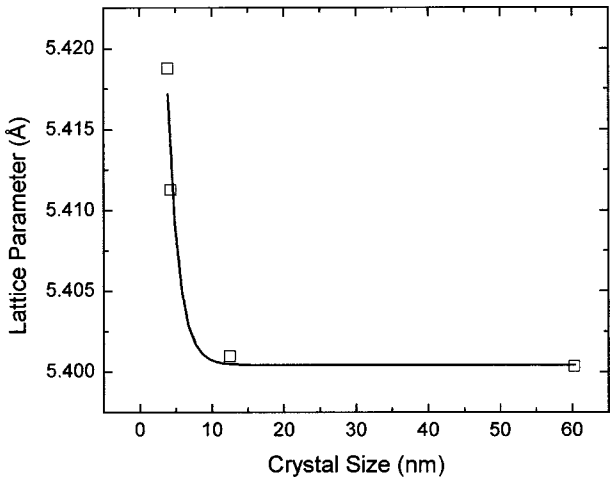

FIG. 5. The variation of lattice parameter vs crystal size.

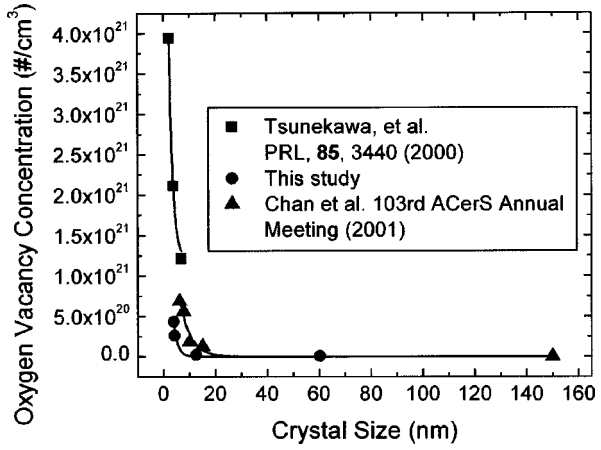

FIG. 6. The variation of oxygen vacancy concentration vs crystal size.

oxygen vacancies, $V_{\mathrm{O}}^{\bullet\bullet}$ (Kroger–Vinger notation). In order to evaluate the defect concentration, the lattice parameter related to the ionic radius was used to fulfill this goal. The Ce^{3+} is assumed to retain the normal coordination number of 8 as that of Ce^{4+} in the unit cell of CeO_2; those defects are assumed to distribute randomly in nanoparticles. The defect reaction for the formation of $V_{\mathrm{O}}^{\bullet\bullet}$ and subsequent Ce^{3+} is given as

$$2\mathrm{Ce}_{\mathrm{Ce}}^{x}+\mathrm{O}_{\mathrm{o}}^{x}=2\mathrm{Ce}_{\mathrm{Ce}}^{\prime}+V_{\mathrm{O}}^{\bullet\bullet}+\tfrac{1}{2}\mathrm{O}_2(\mathrm{gas}). \tag{2}$$

Therefore $[\mathrm{Ce}^{3+}]=2[V_{\mathrm{O}}^{\bullet\bullet}]$. CeO_2 exhibits the fluorite structure ($Fm3m$), so the relationship between the lattice parameter and the ionic size is $\sqrt{3}/4a=r_{\mathrm{Ce}^{4+}}+r_{\mathrm{O}^{2-}}$, where $r_{\mathrm{Ce}^{4+}}$ and $r_{\mathrm{O}^{2-}}$ are the ionic radii of Ce^{4+} and O^{2-}, respectively.[9] If the ratio of $\mathrm{Ce}^{3+}/\mathrm{Ce}^{4+}=c$, the $V_{\mathrm{O}}^{\bullet\bullet}/\mathrm{O}^{2-}$ ratio is $c/4$. The lattice parameter will change to

$$\frac{\sqrt{3}}{4}(a'-a_0)=c\left[r_{\mathrm{Ce}^{3+}}-r_{\mathrm{Ce}^{4+}}+\frac{1}{4}(r_{V_{\mathrm{O}}^{\bullet\bullet}}-r_{\mathrm{O}^{2-}})\right], \tag{3}$$

where $r_{\mathrm{Ce}^{3+}}$ is radius of Ce^{3+}, $r_{V_{\mathrm{O}}^{\bullet\bullet}}$ is the oxygen vacancy radius, a' is the new lattice parameter. The sizes of the ions were taken to be $r_{\mathrm{Ce}^{3+}}=0.1283$ nm,[10] $r_{\mathrm{Ce}^{4+}}=0.1098$ nm,[10] $r_{\mathrm{O}^{2-}}=0.124$ nm[10] and $r_{V_{\mathrm{O}}^{\bullet\bullet}}=0.138$ nm.[11] Using the measured lattice parameters then, the $[V_{\mathrm{O}}^{\bullet\bullet}]$ was calculated (Fig. 6). The $[V_{\mathrm{O}}^{\bullet\bullet}]$ was $\approx 4\times10^{20}/\mathrm{cm}^3$ (1.7%) in the 4.6 nm single crystals and decreased to $\approx 7.2\times10^{18}/\mathrm{cm}^3$ (0.028%) in the 60 nm single crystals. Very recently, Chan *et al.*[12] proposed lattice expansion in nanometer ceria particle; those data are also shown in Fig. 6.

In summary, the size-induced lattice relaxation in nanocrystalline CeO_2 was observed by x-ray diffraction and TEM lattice images. The effects of size and strain on the diffraction line broadening were separated. Size contributes to the line broadening for the fine crystals (<5 nm) while strain effect became significant for larger crystals. The shift in lattice parameters with crystal size was assumed to be due to the formation of oxygen vacancies and the associated Ce^{3+}. This model shows that the concentration of oxygen vacancies changed≈two orders of magnitude when the crystal size increased from 4 to 60 nm.

[1] A. P. Alivisatos, J. Phys. Chem. **100**, 13226 (1996).
[2] K. Ishikawa and T. Uemori, Phys. Rev. B **60**, 11841 (1999).
[3] V. R. Palkar, P. Ayyub, S. Chattopadhyay, and M. Multani, Phys. Rev. B **53**, 2167 (1996).
[4] S. Tsunekawa, R. Sivamohan, S. Ito, A. Kasuya, and T. Fukuda, Nanostruct. Mater. **11**, 141 (1999).
[5] J. R. McBride, K. C. Hass, B. D. Poindexter, and W. H. Weber, J. Appl. Phys. **76**, 2435 (1994).
[6] X. D. Zhou and W. Huebner (unpublished).
[7] H. P. Klug and L. E. Alexander, *X-Ray Diffraction Procedure*, 2nd ed. (Wiley, New York, 1974).
[8] S. Tsunekawa, K. Ishikawa, Z.-Q. Li, Y. Kawazoe, and A. Kasuya, Phys. Rev. Lett. **85**, 3440 (2000).
[9] D. E. Sands, *Introduction to Crystallography* (Dover, New York, 1993).
[10] R. D. Shannon, Acta Crystallogr., Sect. A: Cryst. Phys., Diffr., Theor. Gen. Crystallogr. **A32**, 751 (1976).
[11] S. J. Hong and A. V. Virkar, J. Am. Ceram. Soc. **78**, 433 (1995).
[12] S.-W. Chan, F. Zhang, E. Apak, J. Spenier, and I. P. Herman (unpublished).